Green Chemistry

PAPER

View Article Online
View Journal

Cite this: DOI: 10.1039/d6gc01695b

Depolymerized lignin as an enabler for superior lignin–acrylonitrile copolymers for sustainable wet-spun fibers

Talita Nascimento,[a] Marta Ramos-Andrés, *[a,b] Marta C. Lourenço[a] and Ana C. Marques *[c]

The growing demand for renewable materials and the valorization of biomass by-products have positioned lignin as a promising raw material for bio-based carbon fiber (CF) production. However, its heterogeneous, branched structure, and multiple functional groups often yield polymers with irregular architectures, limiting CF mechanical performance. To address this, LignoBoost lignin (LB) was subjected to acidic oxidative depolymerization, generating a depolymerized lignin fraction (DLB) with a controlled number of reactive sites. DLB was subsequently copolymerized with non-fossil acrylonitrile (AN) through a two-step aqueous free-radical process, without prior chemical functionalization. The effect of the initiation system was evaluated using APS/$NaHSO_3$/$FeSO_4$, $CaCl_2$/H_2O_2, and a dual-initiator approach, revealing a synergistic effect that enabled the synthesis of high molecular-weight copolymers with optimized structural properties. Copolymers were synthesized with 0 to 50 wt% DLB and characterized alongside polyacrylonitrile (PAN) using GPC, EA, ATR–FTIR, ^{1}H NMR, ^{31}P NMR, TGA, and DSC. Successful copolymer formation was confirmed, with the extent of incorporation fraction and conversion quantified. Increasing DLB content resulted in improved thermal stability, reflected in higher char yield (30–36% for AN-DLB copolymers *vs.* 27% for PAN, at *ca.* 900 °C) and a more controlled, safer cyclization pathway, which is an essential requirement for CF precursor processing. Comparison with copolymers prepared from native LB demonstrated clear advantages of depolymerization: AN–DLB copolymers exhibited higher M_n (81 868 g mol^{-1} *vs.* 15 588 g mol^{-1}), narrower dispersity ($Đ$ = 1.98 *vs.* 2.10), thermal transitions more closely resembling PAN, and superior structural integrity when processed into wet-spun fibers. Overall, oxidative depolymerization significantly enhances lignin's compatibility in AN-based copolymers, revealing the potential of poly(AN–DLB) to serve as a sustainable precursor for next-generation carbon fibers.

Received 20th March 2026,
Accepted 13th April 2026

DOI: 10.1039/d6gc01695b

rsc.li/greenchem

Green foundation

1. This work advances green chemistry by demonstrating that low-temperature acidic oxidative depolymerization (no organic solvents, catalysts or pressure) produces lignin with reduced phenolic OH content and ~one reactive site per molecule, enabling the synthesis of more linear lignin–AN copolymers without multi-step chlorinated functionalization routes. Copolymerization proceeds in aqueous medium, without azo-initiators, incorporating up to 50 wt% lignin to produce sustainable, high-quality wet-spun precursor fibers.
2. Depolymerized LignoBoost lignin (DLB) yields copolymers with higher M_n, narrower $Đ$, enhanced thermal stability, safer cyclization, and excellent processability into continuous fibers relative to both PAN and copolymers of untreated lignin. Eliminating acrylation/acetylation sequences gives the same reactivity benefit while reducing hazardous reagents and processing steps, improving renewable carbon integration.
3. Greenness can increase further by replacing the solvents used for purification and fiber spinning with greener alternatives, scaling continuous depolymerization and copolymerization, and optimizing the subsequent stabilization and carbonization steps for a fully renewable carbon fiber route.

[a]*Centro de Recursos Naturais e Ambiente (CERENA), Instituto Superior Técnico, Universidade de Lisboa, Avenida Rovisco Pais, 1049-001 Lisbon, Portugal. E-mail: marta.ramos@uva.es*
[b]*Bioeconomy Institute of the University of Valladolid (BioEcoUVa), PressTech Group, Department of Chemical Engineering and Environmental Technology, School of Industrial Engineering, University of Valladolid, Paseo Prado de la Magdalena 3-5, 47011 Valladolid, Spain*
[c]*CERENA, Department of Chemical Engineering, Instituto Superior Técnico, Universidade de Lisboa, Avenida Rovisco Pais, 1049-001 Lisbon, Portugal. E-mail: ana.marques@tecnico.ulisboa.pt*

1. Introduction

Carbon fiber (CF) is a lightweight material made of polymeric precursors or carbon allotrope building blocks possessing superior tensile strength, durability, extraordinarily low weight, excellent thermal and electrical properties, high chemical resistance and good temperature tolerance.[1,2] Due to these characteristics, CF has been applied in several industries such as automotive, high-end sporting goods, military, construction, wind energy, aerospace, thermoplastic compounding, and 3D printing.[3–5]

Commercial CFs are mainly (about 95%) produced from polyacrylonitrile (PAN) based precursors because of their capability to achieve high carbon yield and high-performance CFs.[6] However, PAN is an expensive petroleum-derived precursor, responsible for about 51% of the total cost of CFs. The material yield, the toxicity of the solvent, and the costly manufacturing stages encourage the search for alternative precursors that are more suitable from technical, economic, and environmental perspectives.[7,8] A renewable raw material with high potential as a CF precursor is lignin, the second most abundant biopolymer in lignocellulosic biomass.[9,10] Lignin is a complex aromatic compound that must be removed in the pulp and paper industry, as well as in other biorefineries such as bioethanol production. The majority of the removed lignin is burned for energy recovery or treated as a low-value by-product, resulting in environmental pollution and the waste of a renewable resource. Only a small portion, approximately 2%, is used in the production of value-added products.[11,12] Consequently, the utilization of lignin as a CF precursor presents a means to enhance the value of a by-product that has traditionally been discarded.

To substitute acrylonitrile (AN) and reduce costs while enhancing sustainability, studies have investigated blends of PAN and lignin, achieving acceptable mechanical properties. However, the lignin content is limited because, during thermal treatment, it can generate macro-voids and other defects in the CF due to the lack of chemical bonding.[13,14]

One approach for utilizing lignin as a CF precursor is its radical copolymerization with AN, which can enhance thermal stability during the conversion into a carbon material.[15,16] Xia *et al.* (2016) esterified lignosulfonate with acryloyl chloride to introduce polymerizable vinyl (C═C) groups, enabling free radical copolymerization (FRP) with AN.[17] The resulting lignin–AN copolymers could be spun and thermally stabilized to produce defect-free fibers. Similarly, Liu *et al.* (2020) functionalized aminated lignin using 2-chloroacrylonitrile before copolymerizing it with AN FRP, forming a PAN–lignin copolymer.[18] In both studies, the presence of lignin improved copolymer dispersity and solubility; however, lignin reactivity toward AN was only achievable after prior chemical functionalization. These strategies rely on chloro-derived agents, which are highly toxic and raise concerns regarding process sustainability and scalability.

Strategies involving lignin without further modification have been explored to synthesize PAN–lignin copolymers, including a two-step FRP technique.[19–21] In the first step, AN was polymerized in the presence of the initiator 2,2-azobisisobutyronitrile (AIBN). In the second step, the polymerized AN was introduced into a DMSO solution containing lignin that had been previously activated by a redox reaction involving hydrogen peroxide and chloride ions. These studies demonstrated that the incorporation of lignin into the copolymer lowered the initiation temperature of the cyclization reaction, thereby facilitating more controlled cyclization.[21] The PAN–lignin copolymer also exhibited superior thermal stability compared to the PAN homopolymer.[19] However, these approaches relied on azo-type radical initiators and organic solvent systems, which are less desirable for scale-up, sustainability, and process safety.

Another approach consisted of AN grafting from lignin,[16] instead of grafting PAN onto lignin, also through a two-step FRP process. Optimal lignin concentrations for maximizing carbon yield and thermal properties, compared to PAN, were 15 wt% and 25 wt%, respectively. Moreover, even with a reduction in the molar mass of the AN–lignin copolymer, observed in this work,[16] the carbon yield remained similar to that using PAN.

Given the branched nature of lignin and the abundance of functional groups, most of the polymers synthesized from this material exhibit multi-arm structures, with interesting applications as emulsifiers[22] or carriers.[23] However, lignin-based CFs typically exhibit poor mechanical performance, largely due to the absence of a well-defined and orientation-capable molecular architecture in lignin, and it has been concluded that CF precursor polymer chains must be organized prior to stabilization and carbonization treatments.[24] Orientability refers to the ability of a polymer melt or solution to develop flow-induced anisotropy during extrusion, aligning load-bearing molecular segments along the fiber axis.

So, enhancing chain orientability in lignin-based precursors using simple and cost-effective strategies is essential for enabling the production of high-quality, low-cost CFs. This is a current challenge that has only recently begun to be addressed. In this sense, "deconstruction followed by reconstruction" approaches have been employed by using low molecular-weight lignin bio-oil (*ca.* 600 g mol^{-1}) as a feedstock for polymer synthesis through reversible addition–fragmentation chain transfer (RAFT) polymerization.[1,25] This method has been claimed to enhance chain orientability, resulting in CFs with an average tensile strength of 1.70 GPa and a tensile modulus of 182 GPa.[1] It should be stressed that these authors used lignin bio-oil obtained by red oak pyrolysis in a fluidized bed reactor, which is an extra step involving high temperatures. Moreover, such bio-oil was then functionalized using acryloyl chloride, which displays significant toxicological and environmental risk profiles.

In this context, depolymerization, if properly managed from a sustainability point of view, emerges as a crucial step in lignin-based fiber synthesis, as it generates valuable aromatic compounds that serve as low molecular-weight feedstocks potentially suitable for fiber production. This improvement is

mainly attributed to the presence of more accessible reactive sites (*i.e.*, lower steric hindrance), a lower number of reactive sites per molecule (*i.e.*, reduced branching, leading to more linear structures), and the lower dispersity and greater solubility of depolymerized lignin compared to native lignin.[26,27]

Currently, no studies have focused on the application of depolymerized lignin, without additional functionalization, as a monomer/oligomer in the production of AN–lignin copolymers *via* FRP for fiber synthesis. To address this gap, this work aimed to partially substitute AN monomers with depolymerized LignoBoost lignin (DLB) in AN–DLB copolymers and to investigate the effect of the initial DLB content on the copolymer properties.

Starting from LignoBoost lignin (LB) provides several advantages for this work. It offers a relatively low-ash, industrial-grade lignin with consistent composition, improving reproducibility and chemical control during copolymerization. Unlike crude technical lignins, LB is already purified at scale through an established industrial process, making it both cost-effective and realistic for deployment in emerging value chains. Its use aligns with circular economy principles since lignin is derived from a pulp-mill by-product.

The benefits of lignin depolymerization are demonstrated in this work by directly comparing copolymers synthesized from depolymerized and untreated lignin. In addition, because the copolymerization proceeded in two stages, the contribution of each initiator is evaluated independently, confirming that both are required for optimized structural properties. Furthermore, the practical processability of these materials is validated through the successful fabrication of continuous wet-spun precursor fibers. Overall, the process is designed to be more sustainable than previously reported approaches by using LB lignin as a renewable starting material and non-fossil derived AN, performing the copolymerization in water, avoiding azo-based initiators, and eliminating hazardous functionalization steps.

2. Materials and methods

2.1 Materials

LB obtained from kraft pulping of *Eucalyptus globulus* wood, through the LignoBoost process, was kindly supplied by RAIZ – Forest and Paper Research Institute (Portugal). AN (named Econitrile) was supplied by AnQore (Netherlands). Econitrile is a commercially available, sustainable acrylonitrile produced on a mass-balance basis from non-fossil feedstocks, specifically bio-based and/or circular propylene and ammonia. By utilizing these sustainable production pathways, Econitrile exhibits a carbon footprint at least 60% lower than that of fossil-based acrylonitrile, making it a highly sustainable alternative for polymer synthesis.

Poly(acrylonitrile-*co*-vinyl acetate) [poly(AN–VA)] was kindly supplied by SGL Composites S.A.

Calcium chloride dihydrate ($CaCl_2{\cdot}2H_2O$, Sigma-Aldrich), non-stabilized hydrogen peroxide aqueous solution (H_2O_2, 30% w/v, Panreac), ammonium persulfate (APS, 98%, Thermo Scientific), sodium bisulfite ($NaHSO_3$, Sigma-Aldrich), iron(II) sulfate heptahydrate ($FeSO_4{\cdot}7H_2O$, Panreac), methanol (MeOH, HPLC grade, Fisher Chemical), tetrahydrofuran (THF, HPLC grade, Fisher Chemical), *N*,*N*-dimethylformamide (DMF, HPLC grade, Carlo Erba), lithium chloride (LiCl, extra pure, Riedel-de Haën), dimethyl sulfoxide-d6 (DMSO-d6, for NMR, Thermo Scientific), chloroform-d (for NMR, Thermo Scientific), cholesterol (Sigma-Aldrich), chromium(III) 2,4-pentanedionate ($Cr(acac)_3$, Sigma-Aldrich), pyridine anhydrous (Sigma-Aldrich), and 2-chloro-4,4,5,5-tetramethyl-1,3,2-dioxaphospholane (TMDP, Sigma-Aldrich) were used as received. Aqueous solutions of sodium hydroxide (NaOH, 0.2 M and 1 M) and sulfuric acid (H_2SO_4, 0.1 M and 1 M) were prepared for pH adjustment.

Note: Although AN is recognized as a hazardous monomer, it is still the reference material in commercial carbon fiber production. For this reason, AN was maintained in the formulation to preserve industrial relevance, while the sustainability of the system was enhanced by (i) employing non-fossil derived AN, (ii) significantly increasing the renewable lignin fraction, and (iii) performing copolymerization entirely in water and without azo-based initiators or chlorinated activation chemistries. This approach supports a transition pathway that can be implemented in existing precursor manufacturing chains rather than requiring a disruptive process replacement. DMF and THF were only used during analytical characterization and fiber spinning and never as reaction media. Future process development should focus on replacing these solvents with greener alternatives to further reduce environmental impact.

2.2 Acidic oxidative depolymerization of LB

Following the method described in our previous work,[28] LB (75 g) was mixed with an aqueous H_2O_2 solution (30% w/v, 250 mL) at room temperature (approximately 20 °C) for 5 minutes, forming a naturally acidic suspension with a pH of approximately 1. Depolymerization was carried out in a jacketed glass reactor (LF100, LENZ) equipped with a condenser, a heating recirculating bath (Haake D1 L), and a mechanical stirrer set to 300 rpm (DLH, VELP Scientifica). The reaction was initiated by heating the system at 60 °C and allowed to proceed for 3 h. Upon completion, the sample was dried at room temperature (approximately 20 °C) for 24 h in Petri dishes, followed by drying in an oven at 40 °C for approximately 2 h. At the end, DLB was obtained.

2.3 Synthesis of poly(AN–DLB) copolymers *via* free radical copolymerization

The synthesis was conducted in two sequential stages: (i) generation of radical-active sites on DLB and (ii) suspension copolymerization with AN. The copolymers were synthesized by varying initial DLB content (0–50 wt%).

In the first step, a mixture of $CaCl_2$ (0.67 × DLB mass) and distilled water (8 mL) was added to a 25 mL Schlenk flask equipped with a PTFE stir bar and a rubber septum. After the $CaCl_2$ dissolved, the required amount of DLB (0–3.1 g, Table 1)

Table 1 Copolymers synthesized

	Comonomers			
	DLB/LB		AN	
Copolymer name	wt%	g	wt%	g
PAN	0	0	100	6.2
Poly(AN–DLB)-3.4	3.4	0.2	96.6	6.0
Poly(AN–DLB)-17.5	17.5	1.1	82.5	5.1
Poly(AN–DLB)-33	33.0	2.1	67.0	4.1
Poly(AN–DLB)-50	50.0	3.1	50.0	3.1
Poly(AN–DLB)-17.5(APS)	17.5	1.1	82.5	5.1
Poly(AN–DLB)-17.5($CaCl_2$/H_2O_2)	17.5	1.1	82.5	5.1
Poly(AN–LB)-17.5	17.5	1.1	82.5	5.1

DLB: depolymerized LignoBoost lignin, LB: LignoBoost lignin, APS: ammonium persulfate, AN: acrylonitrile, PAN: polyacrylonitrile.

was added to the mixture, and the system was purged using ultrapure nitrogen (N_2) for 5 minutes at room temperature while stirring at 300 rpm. Following degassing, the appropriate volume (mL) of 30% w/v H_2O_2 (0.37 × DLB mass) was added, and the flask was placed in a preheated oil bath at 55 °C. The activation was carried out under N_2 at 55 °C and 300 rpm for 2 h. At the end of the reaction, the pH of the mixture was adjusted to 3.0 using 1 M NaOH, and the activated DLB (ActDLB) was obtained.

In the second step, copolymerization was performed as a suspension polymerization using water as the reaction medium. Distilled water (8 mL) was added to a 250 mL round-bottomed glass reactor equipped with a condenser, a PTFE stir bar, and a rubber septum. The reactor was placed in a pre-heated oil bath at 55 °C, and pH was adjusted to 3.0 using 0.1 M H_2SO_4. The system was left for 10 minutes under stirring at 300 rpm under a N_2 atmosphere. Then, a concentrated solution of $FeSO_4{\cdot}7H_2O$ was prepared in distilled water, and 2 μL of this solution was added to the reactor (Fe: 0.7 ppm relative to the total DLB + AN mass), followed by stirring for 5 minutes at 200 rpm under N_2. Solutions of APS (0.32% of the total DLB + AN mass) and $NaHSO_3$ (1.694 × APS mass) were separately prepared in distilled water (0.25 mL each), added to the reactor, and stirred for an additional 5 minutes under the same conditions. Next, the required amount of AN (3.1–6.2 g, Table 1) was added to the reactor. Immediately after AN began to polymerize to form PAN, ActDLB was added. The copolymerization reaction was considered complete after 4–5 hours. The resulting mixture was filtered under vacuum and washed with distilled water, and the solid retained on the filter was dried overnight under vacuum.

The AN–DLB copolymers were purified by removing residual unreacted ActDLB through multiple cycles of vortex-assisted extraction using methanol as the solvent. Each extraction cycle was followed by centrifugation, and the process was repeated until the solvent appeared completely colorless (Fig. S1 of the SI).

Copolymers were synthesized with increasing fractions of DLB to partially replace AN, while PAN prepared without DLB served as the reference.

AN was included solely as the industrial benchmark required to assess the technical relevance of the lignin-based copolymers, as PAN remains the dominant precursor for CF production.

The contribution of each initiator was evaluated by performing reactions using APS/$NaHSO_3$/$FeSO_4$ alone or $CaCl_2$/H_2O_2 alone, whereas all other experiments employed both initiators. To assess the relevance of prior depolymerization, an additional copolymer was prepared using untreated LB in place of DLB. The synthesized copolymers are listed in Table 1.

2.4 Spinning dope preparation and the wet-spinning process

The dope preparation process was initiated by dispersing the copolymer in cold DMF (4 °C) to form a fine suspension, preventing gel particle formation and ensuring homogeneous dissolution. The resulting slurry was gradually heated and maintained at 80 °C under continuous stirring for 1 h to yield a highly viscous solution, followed by slow stirring (20 rpm) at 50 °C for 16 h.

Since pure PAN homopolymer is rarely used for industrial wet spinning due to its limited solubility, an industrial-grade poly(AN–VA) copolymer (85 wt% AN, 15 wt% VA) was employed as reference material. The reference spinning dope was prepared at a concentration of 22 wt%. Accordingly, the poly(AN–DLB) dope was prepared at 22 wt%, exhibiting consistency and appearance similar to the reference. In contrast, the poly(AN–LB) dope required a higher concentration (32 wt%) to achieve comparable spinnability. To produce poly(AN–DLB) and poly (AN–LB) dopes, the poly(AN–DLB)-17.5 and poly(AN–LB)-17.5 copolymers were used, respectively.

Fibers were fabricated using a custom wet-spinning line (Fig. S2 of the SI) consisting of a pressure regulator, pneumatic cylinder, spinneret, coagulation bath, washing bath, rollers, and a winding unit. The spinning solution was extruded through a spinneret containing 168 holes (0.127 mm diameter per hole) into a coagulation bath composed of 30 wt% DMF in water. The nascent fibers were subsequently guided through a water washing bath, stretched using rollers, and automatically wound onto bobbins. Finally, the fibers underwent an additional water wash to ensure complete solvent removal and were dried in an oven at 40 °C.

2.5 Characterization

The molecular weight distribution of LB and DLB samples was determined using size exclusion chromatography (HPLC-SEC) with a GPC column (KF-803L; Shodex) protected by a pre-column (KF-G 4A; Shodex). The column was maintained at 40 °C, and THF (HPLC grade) was used as the mobile phase at a flow rate of 1 mL min^{-1}. The molecular weight distribution curves, weight-average molecular weight (M_w), number average molecular weight (M_n), and dispersity index ($Đ$) were obtained using a UV detector (UV-4070, 280 nm). The calibration curve was constructed using polystyrene standards ranging from 266 to 62 500 Da (Agilent) and an ethylbenzene standard of 106 Da (Ehrenstorfer). LB and DLB samples were dissolved in THF at a

concentration of 1 mg mL^{-1} and filtered before analysis (0.45 μm, PTFE).

The molecular weight distribution of the copolymer samples was determined using the same technique but with two GPC columns in series (GRAM 30 Å/1000 Å, PSS, 10 μm) protected by a precolumn (GRAM, PSS, 10 μm) operated at 70 °C. DMF/0.05 M LiCl was used as a mobile phase at a flow rate of 0.6 mL min^{-1}. The M_w, M_n, and $Đ$ values were determined using a RI detector, and the molecular weight distribution curves were obtained using a UV detector. The calibration curve was constructed using the RI detector and poly (methyl methacrylate) (PMMA) standards ranging from 800 to 2 200 000 Da. Copolymer samples were dissolved in DMF/0.05 M LiCl at a concentration of 1 mg mL^{-1} and then filtered (0.45 μm, PTFE). The proportion of monomers, dimers and trimers was estimated following the method previously described by Lourenço *et al.* (2025).[28]

The analysis of the functional groups was performed using attenuated total reflectance (ATR)–Fourier transform infrared spectroscopy (FTIR) with a Spectrum Two FT-IR spectrometer (PerkinElmer) equipped with a UATR accessory. Approximately 5 mg of the solid sample was placed directly on the diamond ATR crystal and gently pressed with a flat-tip anvil to ensure optimal contact. Transmittance spectra were recorded in the wavenumber range of 4000–900 cm^{-1}, with a resolution of 4 cm^{-1} and 16 scans per sample.

Thermogravimetric analysis (TGA) and derivative thermogravimetry (DTG) were carried out using a Hitachi STA7200 TGA/SDTA analyzer from Melter Toledo. Approximately 5 mg of each sample was placed in an alumina pan and heated at a rate of 10 °C min^{-1} under a N_2 atmosphere (200 mL min^{-1}) from 35 to 900 °C.

Differential scanning calorimetry (DSC) analyses were performed using a DSC 4000 instrument. Approximately 7 mg of each sample was placed in an aluminum pan and then heated from 30 to approximately 400 °C at a rate of 10 °C min^{-1} under air and N_2 atmospheres, each at a flow rate of 20 mL min^{-1}.

Elemental analysis (EA) of LB, DLB, and the copolymers was performed using an EMA 502 elemental analyzer to determine the carbon, hydrogen, nitrogen, and sulfur contents. The oxygen content was estimated using mass balance, subtracting the other percentages from 100%. The empirical formula of the phenylpropane unit (PPU) of LB and DLB was calculated from the EA results and from the methoxy group content determined using ^{1}H NMR, following the method described by Sameni *et al.* (2016).[29] The overall conversions and incorporation fractions of AN and DLB into the copolymers were also estimated from EA. The detailed mathematical equations used to calculate these parameters are given in the SI (eqn (S1)–(S4)). Briefly, since the nitrogen content in the lignin structure can be considered negligible, the incorporation fraction of AN was determined by comparing the nitrogen content of the copolymer to that of the pure PAN homopolymer. The individual monomer conversions were subsequently calculated using a mass balance approach based on the mass of the final purified yield and the initial monomer feed.

A Bruker Avance III 400 spectrometer (Karlsruhe, Germany) was used to conduct ^{1}H NMR and ^{31}P NMR analyses. For ^{1}H NMR, 50 mg of dry samples was dissolved in 1 mL of DMSO-d6, and the solution was stirred for 60 min in an ultrasonic bath. ^{1}H NMR was used to determine the content of aromatic hydrogen, methoxy-group hydrogen (OCH_3), alkene hydrogen (CH═CH), CH hydrogen, and CH_2 hydrogen. ^{31}P NMR was performed following the methodology described by Meng *et al.* (2019)[30] and was used to determine the phenolic, aliphatic and carboxylic hydroxyl (OH) group contents of LB and DLB.

Optical microscopy (KERN OZP 558, Kern & Sohn, Balingen, Germany) and scanning electron microscopy (SEM, Phenom ProX G6, Thermo Fisher Scientific, Waltham, MA, USA) were used to evaluate the surface morphology and cross-sectional structure of the as-spun fibers. Fiber diameters were determined from the micrographs using ImageJ/Fiji software (version 1.53k) *via* manual tracing, and the results are reported as mean values.

3. Results and discussion

3.1 Chemical and structural characterization of LB and DLB

The chemical and structural characterization of LB and DLB was performed to verify whether the depolymerization process occurred satisfactorily. The main results of the characterization are shown in Table 2.

The LB and DLB molecular weight analysis (Table 2 and Fig. 1A) revealed that the M_w, M_n, and $Đ$ values decreased from 979 g mol^{-1}, 635 g mol^{-1}, and 1.54, respectively, to 464 g mol^{-1}, 350 g mol^{-1}, and 1.32 after the depolymerization process. The chromatogram shows a clear emergence of two peaks located approximately at 180 g mol^{-1} and 307 g mol^{-1}, which can be attributed to monomers and to dimers–trimers, respectively. As a result, the low-molecular-weight fraction (monomers, dimers, and trimers) increased from 57.4 wt% in LB to 92.8 wt% in DLB. These results demonstrate that the depolymerization process efficiently promoted the cleavage of inter-unit linkages of lignin to make them less heterogeneous.

The results of EA show that, after depolymerization, the content of carbon and hydrogen decreased from 57.99% to 43.62% and 5.55% to 3.77%, respectively. This decrease may be associated with the oxidative power of H_2O_2, which initiates the cleavage of methoxy groups through demethoxylation. Nonetheless, the oxygen content increased from 32.86% to 46.63%, reflecting the oxidative nature of the depolymerization process, in which an increase in oxygen content over time is expected. The results derived from the empirical formula of the PPU indicate an increase in PPU size. This may occur because during oxidative depolymerization, inherent functionalization takes place concurrently, altering the size of PPU units in the depolymerized lignin as exhibited in our previous work samples.[27]

^{31}P NMR was used to quantify the OH groups in LB and DLB (Fig. S3 – SI). Following depolymerization, both the phenolic hydroxyl (OHphen) and aliphatic hydroxyl (OHaliph) contents decreased, from 4.31 to 2.96 mmol g^{-1} and from 1.53 to

Table 2 Chemical and structural characterization of LB and DLB

Parameter	LB	DLB
C/H/O/S/N (wt%)	57.99/5.55/32.86/3.10/0.52 ± 0.03/0.02/0.06/0.24/0.33	43.62/3.77/49.63/2.96/0.02 ± 0.07/0.19/0.12/0.01/0.00
Empirical formula of the PPU	$C_9H_{5.944}O_{2.461}S_{0.228}N_{0.087}(OCH_3)_{2.372}$	$C_9H_{6.525}O_{7.470}S_{0.265}N_{0.004}(OCH_3)_{1.431}$
$M_{w,PPU}$ (g mol^{-1})	236	287
M_w (g mol^{-1})	979	464
M_n (g mol^{-1})	635	350
$Đ$	1.54	1.32
Monomers + dimers + trimers (wt%)	57.4	92.8
OHphen (mmol g^{-1})	4.31	2.96
OHaliph (mmol g^{-1})	1.53	1.22
OHcarb (mmol g^{-1})	0.35	3.45
OHphen (mol/mol)	2.74	1.04

LB: LignoBoost lignin, DLB: depolymerized LignoBoost lignin, PPU: phenylpropane unit, $M_{w,PPU}$: molecular weight of the PPU, M_w: weight-average molecular weight, M_n: number-average molecular weight, $Đ$: dispersity index.

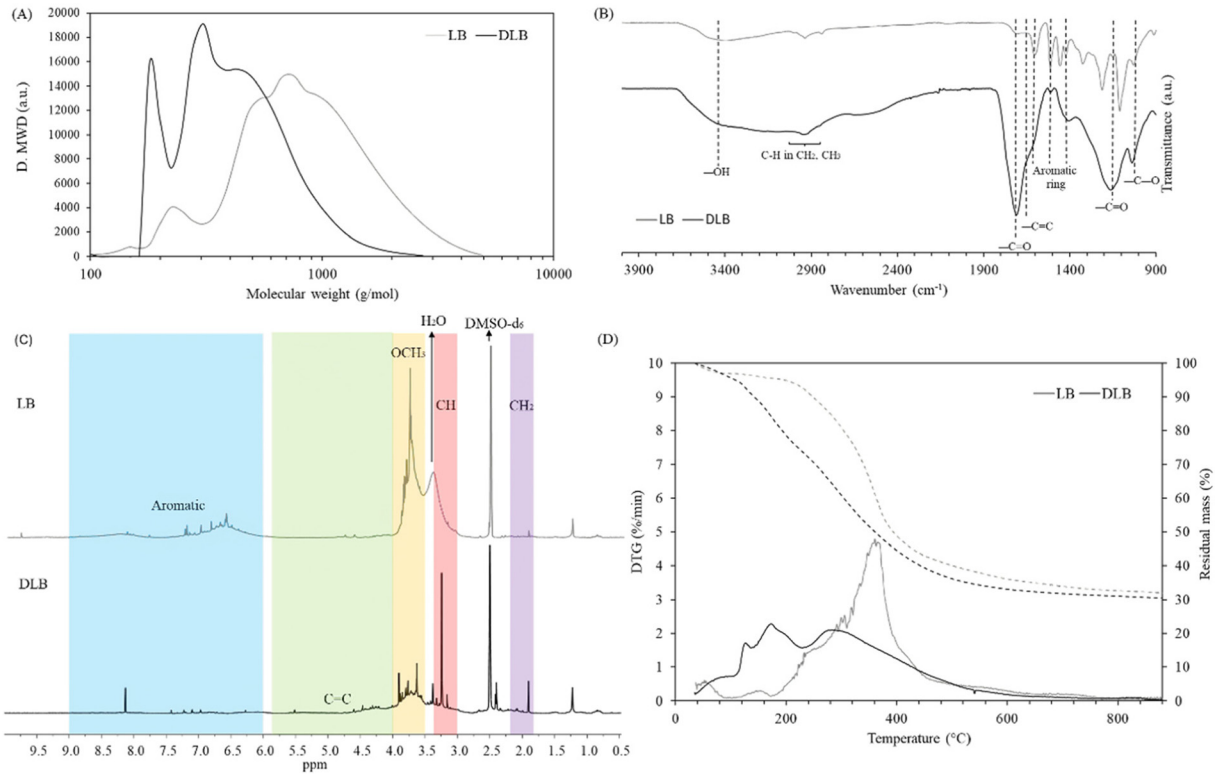

Fig. 1 Chemical and structural characterization of LB and DLB through (A) GPC, (B) ATR–FTIR, (C) ^{1}H NMR, and (D) TGA/DTG.

1.22 mmol g^{-1}, respectively. However, the total OH content increased, primarily due to an increase in carboxylic hydroxyl (OHcarb) groups, which grew from 0.35 to 3.45 mmol g^{-1}. Regarding the OHphen subtypes, the concentrations of syringyl (S) and guaiacyl (G) units decreased from 2.43 to 0.56 mmol g^{-1} and from 0.52 to 0.41 mmol g^{-1}, respectively. In contrast, the content of *p*-hydroxyphenyl (H) units increased from 0.29 to 0.58 mmol g^{-1}. This shift could be associated with demethoxylation occurring during the acidic oxidative depolymerization process. The decrease in OHphen, which are the reactive groups after activation in the copolymerization, led to getting approximately one single reactive site per molecule (Table 2), promoting more linear copolymers in comparison with LB, the latter having 2.74 sites per molecule, which would promote more branched architectures. This is a clear advantage of this particular depolymerization strategy for the production of new linear copolymers to be used for fiber production.

Modifications in the functional groups of DLB compared with those of LB (Fig. 1B) were observed. An increase in the intensity of the band corresponding to OH groups (3600–3000 cm^{-1}) was noted, which agrees with the quantification of OH groups obtained through ^{31}P NMR. The peaks at

2938 and 2842 cm^{-1}, corresponding to the C–H stretching vibrations of methyl (CH_3) and methylene (CH_2) groups, remained visible and broadened, possibly due to the influence of various surrounding functional groups. The peak at 1714 cm^{-1} showed a noticeable increase, indicating a higher content of C=O functional groups, consistent with the substantial increase in OHcarb groups. This phenomenon is related to the oxidation process during depolymerization, which also accounts for the appearance of new C=C groups in the band at 1642 cm^{-1}. The presence of C=C groups in DLB was also confirmed by ^1H NMR, as the spectra (Fig. 1C) show signals in the region of 4.0–5.8 ppm. Additionally, the peaks at 1604, 1515, and 1424 cm^{-1}, associated with aromatic skeleton vibrations, remained in DLB, indicating that the aromaticity of lignin was not completely lost after the depolymerization process. Furthermore, the peaks at 1164 cm^{-1} and 1034 cm^{-1}, attributed to C=O in conjugated ester groups and C–O in primary and secondary alcohols, respectively, exhibited an increase in intensity, the latter likely due to the increased presence of OH groups. The increase in OH and C=O groups, along with the emergence of C=C groups, highlights the functionalization of DLB occurring simultaneously with depolymerization.

The percentages of aromatic (6.0–9.0 ppm), alkene (4.0–5.8 ppm), methoxy (3.5–4.0 ppm), CH (3.0–3.3 ppm), and CH_2 (1.8–2.2 ppm) protons were estimated by integrating the peaks in the ^1H NMR spectra (Fig. 1C). The obtained values were 26.9%, ~0%, 54.5%, 10.2%, and 1.0%, respectively, for LB; and 4.1%, 15.5%, 39.7%, 14.4%, and 6.7%, respectively, for DLB. The decrease in aromatic content indicates that oxidative cleavage of the aromatic rings had occurred, leading to the formation of OHcarb groups as the end products of aromatic ring degradation.[31] Accordingly, ring opening may have led to the oxidation of the phenolic groups to carboxylic acid groups, which explains the decrease in OHphen content.[32] These findings are fully supported by the ^{31}P NMR results (Table 2). Additionally, the methoxy group content decreased, confirming the oxidative action of H_2O_2 under acidic oxidative conditions in cleaving methoxy groups, as also observed in the EA results. This explains the reduction in S and G units observed in the ^{31}P NMR results.

The thermal stability of LB and DLB was analyzed using TGA and DTG under a N_2 atmosphere, as shown in Fig. 1D. The DTG curves reveal an initial decomposition stage (30–140 °C) attributed to moisture loss. In the case of DLB, a distinct peak at 126 °C suggests the evaporation of certain monomeric compounds. The second stage (140–230 °C) corresponds to the volatilization of low-molecular-weight oligomers and functional groups such as carboxylic acids. DLB showed a higher degradation in this range, which can be attributed to its higher OHcarb content, with a pronounced peak observed at 173 °C. In the 230–600 °C range, most of the LB underwent decomposition, mainly associated with the breakdown of C–C bonds and aromatic rings. LB presented a major decomposition peak at 360 °C, while DLB exhibited its peak at a lower temperature (283 °C), reflecting the effect of depolymerization in producing smaller fragments that degrade at lower temperatures. The TG curve of DLB also displayed a downward shift in decomposition temperature, supporting the formation of lower-molecular-weight compounds and the introduction of specific functional groups during depolymerization. At 600 °C, the residual mass was 36% for LB and 30% for DLB, suggesting a slight reduction in thermal stability in DLB, consistent with its lower molecular weight.

3.2 Copolymerization of DLB and AN with increasing initial DLB content

This section examines how varying the initial DLB content affects the molecular weight distribution, DLB incorporation fraction, chemical structure, and thermal behavior of the copolymers.

From the GPC results (Fig. 2), it is possible to observe that PAN and DLB have their size distribution in opposite regions (19.7–29.7 min and 34.1–46.0 min, respectively). The copolymers show size distribution located between these two regions. Although the molecular weight calculations were performed using the RI detector, the UV detector is suitable for representing the molecular weight distribution because it is more sensitive to compounds that absorb in the UV range, such as aromatics and, consequently, lignin (as seen in the intensity differences between PAN and DLB). Therefore, this detector not only visualizes the molecular weight distribution but also qualitatively indicates the extent of lignin incorporation in the copolymer, which agrees with the quantitative incorporation results presented later. The varying degree of lignin incorporation can also be qualitatively observed through the color of the copolymer solid samples (Fig. S4 – SI).

As observed in Fig. 2 and Table 3, the copolymers exhibit a lower molecular weight as the initial DLB content increases. M_w progressively decreases from 1 549 542 to 5207 g mol^{-1} for 3.4 to 50 wt% initial DLB content, respectively. The presence of a higher concentration of activated DLB in the system provides a correspondingly greater number of reactive macro-radicals ($DLB^{\bullet}$). Consequently, growing PAN $^{\bullet}$ chains have a much higher probability of encountering these sites early in their

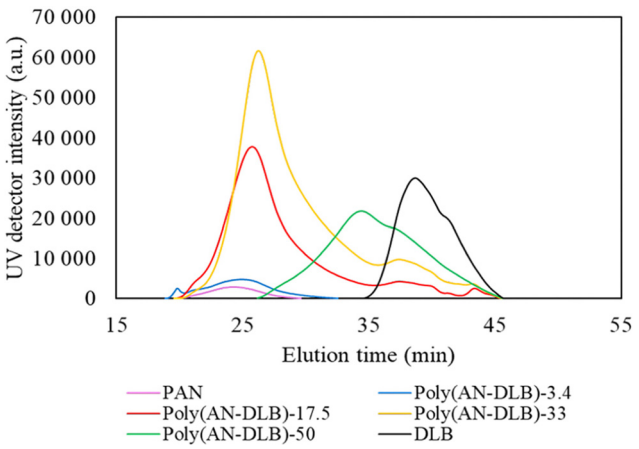

Fig. 2 Molecular weight distribution of PAN, copolymers, and DLB.

Table 3 Molecular weight of PAN, copolymers, and DLB

	Average molecular weight (g mol^{-1})		
Copolymers	M_w	M_n	$Đ$
PAN	621 357	202 443	3.07
Poly(AN–DLB)-3.4	1 549 542	352 995	4.39
Poly(AN–DLB)-17.5	161 975	81 868	1.98
Poly(AN–DLB)-33	83 866	30 424	2.76
Poly(AN–DLB)-50	5 207	3 543	1.47
DLB	464	350	1.32

PAN: polyacrylonitrile, AN: acrylonitrile, DLB: depolymerized LignoBoost lignin, M_w: weight-average molecular weight, M_n: number-average molecular weight, $Đ$: dispersity index.

propagation phase, leading to premature termination *via* radical–radical coupling. This results in significantly shorter chains and a lower overall molecular weight. This phenomenon was also observed by Oliveira *et al.* (2020), who reported that the M_w of their AN-Kraft lignin (KL) copolymer decreased progressively from 285 500 g mol^{-1} to approximately 39 690 g mol^{-1}, which they attributed to an increase in available macro-radical sites (KL$^{\bullet}$).[16] It is also worth noting a certain homogeneity in the copolymers, which show $Đ$ values generally lower than those of PAN (1.47–2.76 *vs.* 3.07).

Surprisingly, the copolymer poly(AN–DLB)-3.4 exhibits a much higher M_w than PAN (1 549 542 *vs.* 621 357 g mol^{-1}). At very low DLB content (3.4 wt%), the system is heavily dominated by AN propagation, allowing PAN macro-radicals to grow freely to larger sizes. Considering the low average functionality of DLB (~1.04 OHphen per molecule, Table 2), occasionally an activated DLB molecule can act as a bi-functional coupling agent between two of these long, growing PAN chains. This sequential termination creates a linear macromolecular bridge (PAN–DLB–PAN), which effectively doubles the molecular weight of the resulting chains without forming an insoluble crosslinking network. Consequently, the dispersity of poly(AN–DLB)-3.4 is also higher than that of PAN (4.39 *vs.* 3.07).

EA of the copolymers in terms of C, H, O, and S content (in percent) was analyzed (Table 4).

The EA results show that the carbon content is higher in PAN (66.97 wt%) than in DLB (43.62 wt%), as expected due to the acidic oxidative depolymerization applied to LB. This trend is also reflected in the copolymers, where the carbon content decreases from 64.90 wt% in poly(AN–DLB)-3.4 to 44.68 wt% in poly(AN–DLB)-50. All the copolymers contain sulfur and oxygen. Since the PAN homopolymer does not contain either of these elements, their presence confirms that DLB—which contains both in its structure—was incorporated into the copolymers. Additionally, DLB contains only a negligible amount of nitrogen; therefore, the nitrogen detected in the copolymers originates from the PAN component and was used to estimate the incorporation fraction of DLB and AN. It is also important to note that as the DLB content in the copolymer increases, sulfur and oxygen contents increase while the nitrogen content decreases. This indicates that higher initial amounts of DLB lead to a greater DLB incorporation fraction in the final copolymer. This interpretation is supported by the calculated mass conversions, which represent the fraction of each comonomer that reacted to form the copolymer, whereas the incorporation fraction values represent the actual proportion of each comonomer in the copolymer structure. The results are presented in Fig. 3.

It can be observed that as the initial DLB content increases, the conversions of both AN and DLB also increase. However, when the initial DLB content exceeds 33 wt%, the conversions of both monomers decrease. In the case of DLB, the decrease is slight (from 39.07 to 27.29%), whereas for AN the drop is much more pronounced (from 43.47 to 6.97%). This behavior suggests that increasing the initial DLB content promotes the formation of a larger number of reactive sites, providing more locations where PAN chains can terminate, which enhances the conversion of both AN and DLB. However, an excessively high initial DLB content (50 wt%) appears to lead to inhibition, likely due to steric hindrance[20] and mass-transfer limitations associated with the solid nature of DLB, which can hinder diffusion during suspension polymerization when present at such a high concentration.

Regarding the incorporation fraction of comonomers into the final copolymer, as the initial DLB content increases (3.5, 17.5, 33 wt%), the incorporation fraction of DLB increases proportionally, with incorporation fraction values very close to the initial DLB concentrations in the reactor (2.5, 17.1, and 31.1 wt%). However, when the initial DLB content is too high (50 wt%), the conversion of AN is negatively affected. As a result, the copolymer exhibits a much higher DLB incorporation fraction than expected (79.6 wt%) and a low total yield due to the low AN conversion.

Table 4 Elemental analysis of PAN, copolymers, and DLB

Copolymers	Nitrogen (%)	Carbon (%)	Hydrogen (%)	Sulfur (%)	Oxygen (%)
PAN	25.92 ± 0.12	66.97 ± 0.18	5.96 ± 0.06	n.d.	n.d.
Poly(AN–DLB)-3.4	25.29 ± 0.04	64.90 ± 0.00	5.51 ± 0.03	0.13 ± 0.08	4.18 ± 0.09
Poly(AN–DLB)-17.5	21.51 ± 0.05	61.57 ± 0.05	5.22 ± 0.06	0.21 ± 0.14	11.51 ± 0.20
Poly(AN–DLB)-33	17.87 ± 0.00	58.04 ± 0.05	5.02 ± 0.01	0.47 ± 0.17	18.60 ± 0.07
Poly(AN–DLB)-50	5.28 ± 0.09	44.68 ± 0.20	4.22 ± 0.04	0.94 ± 0.01	40.53 ± 1.23
DLB	0.02 ± 0.00	43.62 ± 0.07	3.77 ± 0.19	2.96 ± 0.01	49.63 ± 0.12

PAN: polyacrylonitrile, AN: acrylonitrile, DLB: depolymerized LignoBoost lignin.

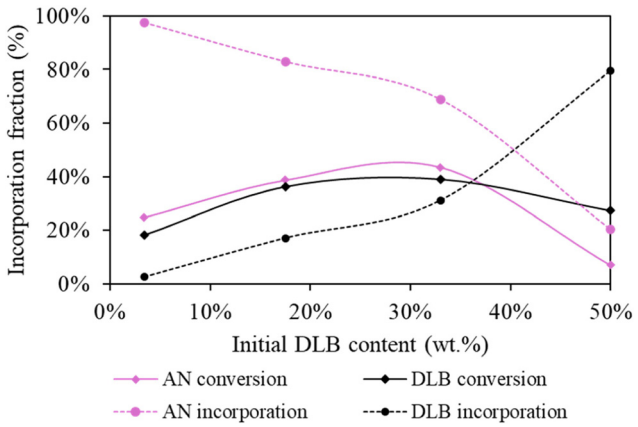

Fig. 3 Mass conversion and incorporation fraction of DLB and AN into copolymers with different initial DLB contents.

ATR–FTIR analysis (Fig. 4) of PAN, DLB, and the resulting copolymers revealed the presence of characteristic functional group signals from both components in the copolymer spectra. The peaks associated with DLB—namely the broad OH stretching band (3600–3000 cm^{-1}), the C=O stretching vibration (1710 cm^{-1}), and the aromatic skeletal vibration (1604 cm^{-1})—were clearly observed in the copolymers. Their relative intensity increased proportionally with the initial DLB content, indicating greater incorporation of DLB into the copolymer structure. Similarly, the copolymers exhibited the characteristic peaks of PAN, including the C≡N stretching band (2244 cm^{-1}), the C–H bending vibrations from CH_2 and CH_3 (1451 cm^{-1}), and the CH groups (1356 cm^{-1}). The relative intensity of these bands increased with higher initial amounts of AN, confirming its contribution to the polymer matrix. The simultaneous presence of both sets of characteristic peaks confirms that the copolymerization process was successfully achieved.

Peaks at 1316 cm^{-1} and 1117 cm^{-1}, which are imperceptible in other copolymers, become highly pronounced in the poly(AN–DLB)-50 copolymer. These bands are not characteristic of PAN, and although they may be present in DLB, they are more likely formed as a result of DLB crosslinking, as demonstrated in our previous work.[28] In poly(AN–DLB)-50, the peak at 1316 cm^{-1} can be attributed to C–O–C stretching vibrations,[33] whereas the band at 1117 cm^{-1} likely corresponds to in-plane C–H deformations in S units. The presence of the C–O–C signal suggests the formation of ether linkages through crosslinking reactions between activated OHphen groups and other reactive sites, with this signal becoming detectable only when DLB is introduced at the highest initial concentrations (50 wt%). ^{1}H NMR quantification of hydrogen in specific functional groups further supports these observations: among all the copolymers, poly(AN–DLB)-50 exhibited the highest proportion of hydrogen in C–O–C environments, followed by PAN-related environments (CH and CH_2 groups), and then DLB-associated environments.

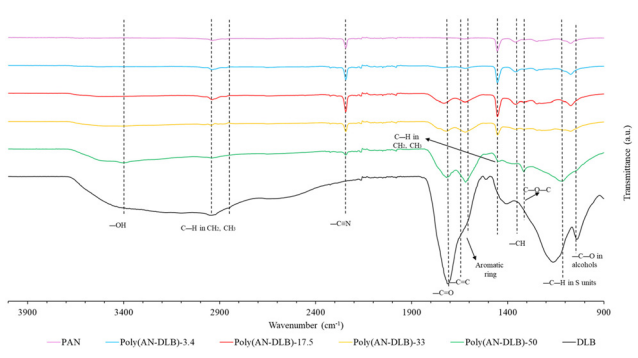

Fig. 4 ATR–FTIR spectra of PAN, copolymers, and DLB.

^{1}H NMR spectra (Fig. S5 of the SI) show that all copolymers exhibited signals in the aromatic region (6.0–9.0 ppm), and as the content of DLB increased, the percentage of protons in this region also increased. Protons in the alkene region (4.0–5.8 ppm) were also observed. Both the aromatic and alkene regions are directly associated with the amount of DLB in the copolymer. The protons in the CH and CH_2 regions were the most abundant in all copolymers, with a significant increase compared to DLB, indicating the presence of PAN chains. Together, the ATR–FTIR and ^{1}H NMR spectra confirm the successful synthesis of poly(AN–DLB) copolymers.

The thermal behavior of the copolymers was investigated using TGA/DTG and DSC analyses under air and N_2 atmospheres. The DTG curves (Fig. 5A) show an initial stage up to 140 °C associated with residual moisture evaporation. The copolymers poly(AN–DLB)-3.4, poly(AN–DLB)-17.5, and poly (AN–DLB)-33 exhibit two major decomposition peaks, one between 290 and 310 °C and another between 400 and 430 °C. As the initial DLB content increases, the intensity of the first peak decreases markedly, suggesting greater incorporation of DLB into the copolymer structure. When the DLB content is moderate (3.4–33 wt%), the DLB is expected to be more uniformly distributed within the PAN matrix, reducing phase separation and preventing the formation of distinct DLB domains.

In contrast, the poly(AN–DLB)-50 copolymer (50 wt% DLB) presents two broader decomposition stages at 267 °C and 347 °C, closely resembling the thermal profile of DLB. This behavior is attributed to the high proportion of DLB in the copolymer. Consequently, poly(AN–DLB)-50 exhibits thermal characteristics more similar to DLB, although with a much higher molecular weight (5207 *vs.* 464 g mol^{-1}). In the TGA curves (Fig. 5A), all copolymers showed progressive mass loss up to 900 °C, with the final residual mass increasing as the initial DLB content increased. This demonstrates lignin's contribution to improved thermal stability in PAN-based copolymers and also reflects the occurrence of DLB crosslinking in poly(AN–DLB)-50, the copolymer with the highest thermal stability. The copolymers exhibited char yield between 30 and 36%, at *ca.* 900 °C, values higher than those of pure PAN (27%) and DLB (30%). This indicates enhanced thermal stability and char yield, supporting their potential as precursors for producing CFs with higher carbon yields than pure PAN.

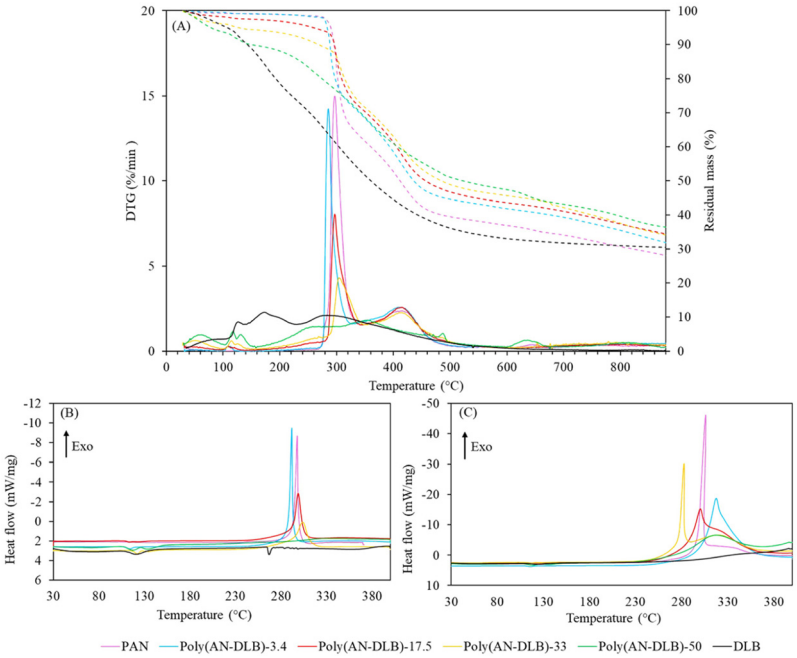

Fig. 5 (A) TGA and DTG of PAN, copolymers, and DLB and DSC curves of PAN, copolymers, and DLB in (B) N_2 and (C) air.

The thermal properties of the synthesized copolymers were also investigated using DSC under both air and N_2 atmospheres. The inclusion of both environments was motivated by the influence of oxidative reactions during the thermal stabilization process of PAN in CF production.

The DSC analysis under N_2 (Fig. 5B) shows that both DLB and all copolymers exhibit an endothermic event between 100 and 150 °C, corresponding to the glass transition temperature. This transition is characterized by a sigmoidal change in the DSC curve.[21] The DSC curve of PAN displays a sharp exothermic peak, with an onset temperature (T_{onset}) at 234.9 °C and a peak temperature (T_{peak}) at 297.9 °C. This exothermic event is attributed to the cyclization of nitrile groups *via* a free radical mechanism occurring in the absence of oxygen, leading to a rapid and intense heat release.[34] A similar exothermic peak is observed in the poly(AN–DLB)-3.4, poly(AN–DLB)-17.5, and poly(AN–DLB)-33 copolymers, although with progressively lower T_{onset} values than with PAN: 235.7, 227.8, and 215.9 °C, respectively. This shift toward lower temperatures indicates that the cyclization process begins earlier in the presence of DLB.

The heat release per temperature interval ($\Delta H/\Delta T$) is a parameter that characterizes the sharpness and intensity of the exothermic peak. $\Delta H/\Delta T$ was calculated by integrating the normalized peak area (ΔH) and dividing it by the corresponding temperature interval (ΔT). As the initial DLB content increases, the cyclization peaks become broader and less intense, with $\Delta H/\Delta T$ values decreasing from −4.9 J g^{-1} $°C^{-1}$ for pure PAN to −4.1, −3.4, and −2.6 J g^{-1} $°C^{-1}$ for poly(AN–DLB)-3.4, poly(AN–DLB)-17.5, and poly(AN–DLB)-33, respectively. This trend indicates slower energy release during the cyclization process, suggesting more controlled and efficient cyclization. Such gradual thermal behavior is desirable, as PAN homopolymers typically exhibit rapid and uncontrolled cyclization, which is one of the key limitations to their carbonization process.[34] To try to solve this, itaconic acid or methyl acrylate is typically used as a comonomer, together with AN. In contrast, the poly(AN–DLB)-50 copolymer does not exhibit any exothermic peak, which is attributed to its low PAN content. Given the complex and amorphous nature of crosslinked DLB, it lacks the capacity for cyclization. As a result, the incorporation of large amounts of DLB into the copolymer suppresses this characteristic thermal transition.

The DSC analysis conducted under an air atmosphere (Fig. 5C) revealed a thermal profile characterized by two distinct exothermic transitions: a sharp, intense peak followed by a shoulder. Although the underlying reactions are complex, literature indicates that cyclization is followed by oxidation. Accordingly, the first exothermic peak is primarily attributed to nitrile cyclization, while the subsequent shoulder corresponds to oxidative reactions.[34,35] As observed under N_2, the incorporation of DLB lowered the T_{onset} values of the cyclization process (216.6–229.6 °C *vs.* 240.3 °C for PAN, Table 5). This trend agrees with previous studies showing that the addition of small amounts of comonomers can reduce the initiation temperature of PAN cyclization under oxidative conditions.[34,36,37] Regarding the oxidation step, the $\Delta H/\Delta T$ values under air were generally higher for the copolymers than for PAN (11.3–24.1 J g^{-1} $°C^{-1}$ *vs.* 18.1 J g^{-1} $°C^{-1}$ for PAN). Interestingly, this increase was more pronounced at lower DLB loadings (Table 5). This behavior may be attributed to interactions between DLB and PAN during thermal oxidation,

Table 5 Peak, onset and endset temperatures, and energy capacity of the PAN, DLB and copolymers measured using DSC

		PAN	Poly(AN–DLB)-3.4	Poly(AN–DLB)-17.5	Poly(AN–DLB)-33	Poly(AN–DLB)-50
N_2	ΔH cyclization (J g^{-1})	−373.2	−315.1	−329.9	−310.7	[a]
	T_{peak} (°C)	297.9	291.9	298.9	304.0	[a]
	T_{onset} (°C)	234.9	235.7	227.8	215.9	[a]
	T_{endset} (°C)	311.8	312.0	324.4	335.7	[a]
	ΔT cycliz. (°C)	76.9	76.3	96.6	119.8	[a]
	$\Delta H/\Delta T$ cycliz. (J g^{-1} °C^{-1})	−4.9	−4.1	−3.4	−2.6	[a]
Air	ΔH cycliz. and/or oxid. (J g^{-1})	−2767.4	−4004.0	−3833.4	−3440.7	−1665.8
	T_{peak} (°C)	305.9	317.3	300.2	282.5	315.3
	T_{onset} (°C)	240.3	229.6	217.2	216.6	224.1
	T_{endset} (°C)	393.4	396.0	392.8	386.2	371.1
	ΔT cycliz. and/or oxid. (°C)	153.1	166.4	175.6	169.5	147.0
	$\Delta H/\Delta T$ cycliz. and/or oxid. (J g^{-1} °C^{-1})	−18.1	−24.1	−21.8	−20.3	−11.3

ΔH: heat release, T_{peak}: peak temperature, T_{onset}: onset temperature, T_{endset}: endset temperature, ΔT: temperature interval, cycliz.: cyclization, oxid.: oxidation. PAN: polyacrylonitrile, AN: acrylonitrile, DLB: depolymerized Lignoboost lignin. [a] No cyclization.

potentially improving the copolymer's suitability as fiber during the carbonization process. However, as the PAN content decreases with higher DLB incorporation, these oxidation-driven interactions are likely reduced, leading to lower overall energy release.

In poly(AN–DLB)-50, cyclization does not occur; thus, only the oxidation process is observed under an air atmosphere. The differences in chemical and structural characteristics between poly(AN–DLB)-50 and PAN suggest that excessively increasing the initial DLB content (50 wt% and above) enhances thermal stability but significantly compromises other copolymer properties, particularly molecular weight and the ability for cyclization. These changes may negatively affect the CFs derived from this material.

3.3 Role of APS/$NaHSO_3$/$FeSO_4$ and $CaCl_2$/H_2O_2 initiators

The copolymerization process involves the use of two initiators: APS/$NaHSO_3$/$FeSO_4$ and $CaCl_2$/H_2O_2. The hypothesis is that the dual-initiator approach relies on two simultaneous processes: the $CaCl_2$/H_2O_2 system is primarily responsible for activating the lignin into active macro-radicals (DLB$^{\bullet}$), while the APS/$NaHSO_3$/$FeSO_4$ system provides the rapid kinetics necessary to simultaneously initiate and propagate long PAN$^{\bullet}$ chains. The final copolymer is successfully formed through the termination step, driven by the recombination of these rapidly growing PAN$^{\bullet}$ chains with the activated DLB$^{\bullet}$ sites. As discussed in previous sections, increasing the initial DLB content results in a lower molecular weight of the copolymer. This effect is likely due to the higher number of available binding sites on the DLB structure, which serve as termination points for growing PAN chains, thereby limiting their propagation.

To elucidate the individual roles of each initiator, two control copolymerizations were conducted under conditions equivalent to those used for poly(AN–DLB)-17.5 (17.5 wt% of DLB), but using each initiator independently. The molecular weight distribution of the copolymer synthesized using APS/$NaHSO_3$/$FeSO_4$ alone, poly(AN–DLB)-17.5(APS) (Fig. 6A), shows

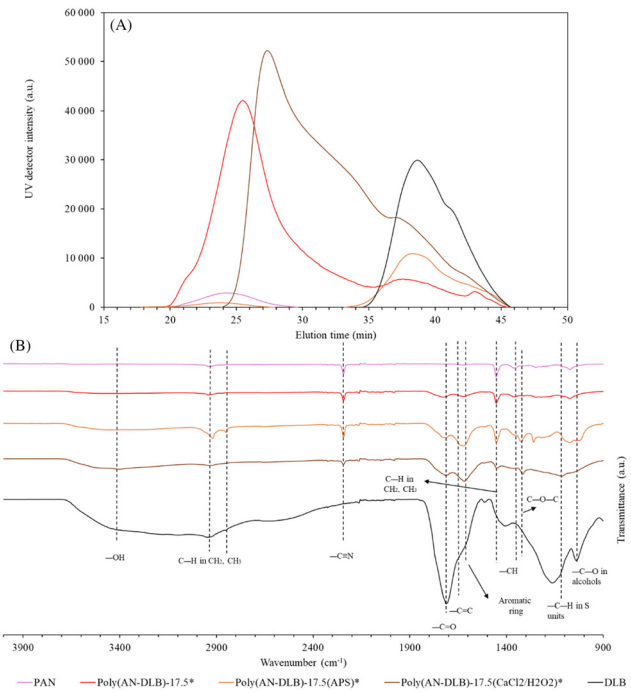

Fig. 6 (A) Molecular weight distribution and (B) ATR–FTIR spectra of PAN, non-purified copolymers, and DLB (* copolymers containing unreacted DLB due to non-purification).

a bimodal profile with two distinct regions corresponding to PAN and DLB. This indicates that, in the absence of $CaCl_2$/H_2O_2, the reactive sites on DLB are not activated, preventing effective copolymerization. In addition, the signal in the PAN region is very low, reflecting an extremely low formation of PAN. This occurs because the non-activated phenolic groups in lignin act as potent radical scavengers, effectively inhibiting the polymerization of AN.

Unlike the previous sample, the molecular weight distribution of poly(AN–DLB)-17.5($CaCl_2$/H_2O_2) (Fig. 6A) exhibits a region between the typical DLB and PAN retention zones,

which is indicative of copolymer formation. This distribution also shows a higher UV detector intensity than that observed for poly(AN-DLB)-17.5, suggesting a greater incorporation of DLB and, consequently, a lower incorporation of AN. In contrast, poly(AN–DLB)-17.5 shows a lower UV signal and elutes at a shorter retention time, consistent with a higher PAN content and a higher molecular weight. This behavior is likely due to the formation of longer PAN chains in the presence of APS/$NaHSO_3$/$FeSO_4$. In the absence of APS/$NaHSO_3$/$FeSO_4$, AN is still able to graft onto activated sites on DLB but cannot propagate into long PAN chains, which reduces the overall molecular weight of the copolymer. It is also important to note that, for comparative purposes, the poly(AN–DLB)-17.5 sample analyzed here corresponds to the unpurified product, which still contains unreacted DLB. As a result, this chromatogram differs slightly from that of the purified version shown in Fig. 2.

The ATR–FTIR spectrum of poly(AN–DLB)-17.5(APS) (Fig. 6B) shows a peak at 2244 cm^{-1}, characteristic of C≡N stretching from PAN. However, this peak appears with much lower intensity compared to the characteristic peaks of DLB: 2950 and 2870 cm^{-1} (C–H in CH_2/CH_3), 1710 cm^{-1} (C═O), and 1604 cm^{-1} (aromatic ring vibrations). This confirms the predominance of DLB in the sample and the low presence of PAN, which—consistent with GPC results—are not chemically bonded. The low PAN homopolymer yield suggested by GPC and ATR–FTIR data is also visually apparent (Fig. S6 of the SI). These findings support the conclusion that in the absence of activation, OHphen groups in DLB act as radical scavengers, significantly inhibiting polymerization.

The limited formation of PAN chains using only $CaCl_2$/H_2O_2 is further supported by the ATR–FTIR results (Fig. 6B). The relative intensity of the C≡N stretching peak at 2244 cm^{-1} is significantly lower than in the poly(AN–DLB)-17.5 spectrum, indicating reduced AN incorporation into the copolymer. Additionally, the OH stretching region (3600–3000 cm^{-1}) displays higher intensity compared to that of poly(AN–DLB)-17.5, confirming a greater presence of DLB relative to PAN in the resulting copolymer.

These results highlight the role of APS/$NaHSO_3$/$FeSO_4$ in promoting PAN chain growth, as well as the role of $CaCl_2$/H_2O_2 in activating reactive sites on DLB and preventing it from acting as a radical scavenger. Together, these initiators enable the formation of high-quality copolymers. The resulting material more closely resembles PAN while benefiting from enhanced properties imparted by lignin.

Based on the experimental results, a schematic representation for the copolymerization of DLB with AN is suggested. During depolymerization (Scheme 1A) the oxidation mecha-

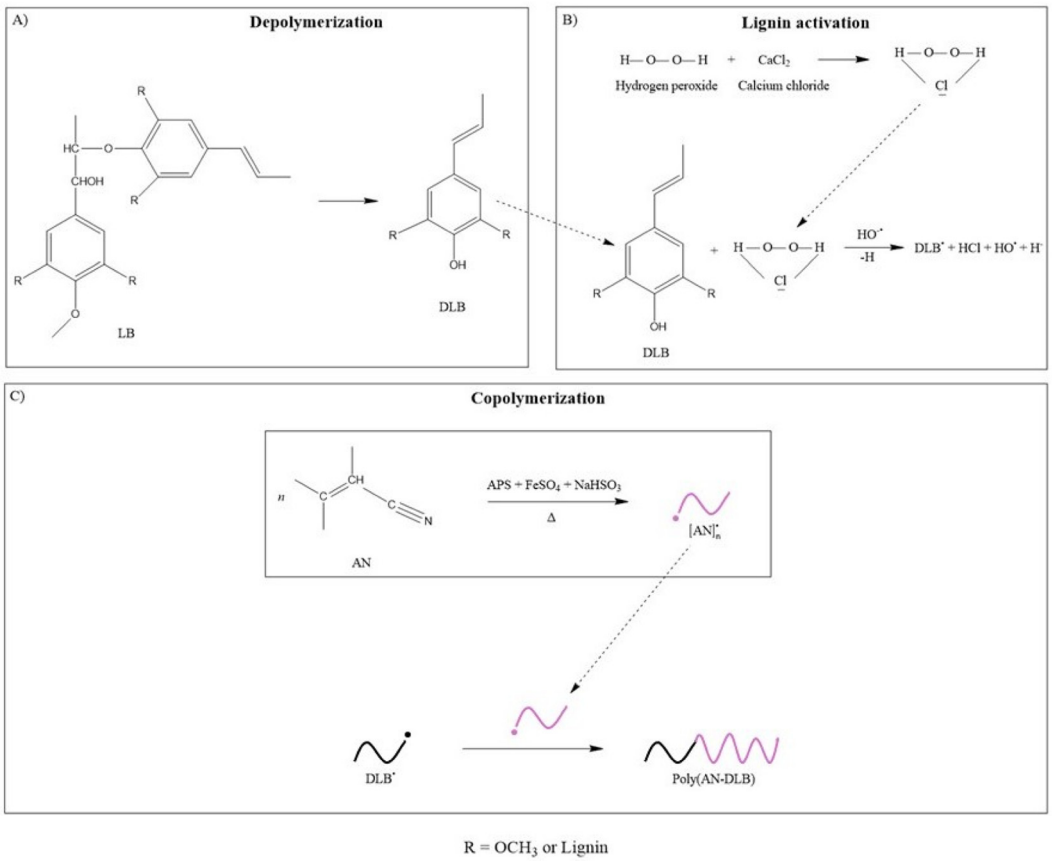

Scheme 1 Schematic representation of (A) LB depolymerization, (B) DLB activation, and (C) PAN propagation and subsequent coupling to produce poly(AN–DLB).

nism of H_2O_2 varies with the pH of the medium. Under the acidic conditions employed in this study, several reaction pathways can describe the interaction between the HO^+ species and lignin. As discussed in our previous works,[27,28] the main mechanisms leading to the formation of various species are (1) aromatic ring hydroxylation, (2) oxidative demethoxylation, (3) oxidative ring cleavage, (4) displacement of side chains, (5) cleavage of beta-aryl ether bonds, and (6) epoxidation. The DLB structure shown in Scheme 1A represents one example of a lignin-derived molecule produced through this depolymerization process.

Following depolymerization, DLB macro-radicals (DLB$^\bullet$) are generated *via* activation by the H_2O_2–$CaCl_2$ redox system, which involves the formation of a hydroperoxide–chloride ion complex (Scheme 1B). The water-soluble initiator (H_2O_2) decomposes upon interaction with the $CaCl_2$–H_2O_2 complex, leading to the formation of hydroxyl radicals (HO$^\bullet$). These radicals can abstract hydrogen atoms from lignin, thereby producing the active DLB$^\bullet$ species.

Simultaneously, the polymerization of AN is efficiently initiated and propagated by the rapid APS/$NaHSO_3$/$FeSO_4$ redox system, generating growing PAN$^\bullet$ macro-radicals (Scheme 1C). Rather than DLB$^\bullet$ acting as the primary initiator for AN, the copolymer is predominantly formed when these rapidly propagating PAN$^\bullet$ chains encounter the activated DLB$^\bullet$ sites, resulting in termination. While general termination in this system may occur *via* chain transfer or disproportionation reactions, the successful synthesis of the poly(AN–DLB) copolymer is mostly driven by the radical–radical coupling between the actively growing PAN$^\bullet$ chains and the resonance-stabilized DLB$^\bullet$ macro-radicals. Therefore, the coupling of the PAN chains can occur either at the oxygen atom (forming an ether linkage) or at the *ortho*/*para* positions of the aromatic ring (forming C–C linkages).

3.4 Role of lignin depolymerization: copolymerization of AN–LB *vs.* AN–DLB

To evaluate the benefits of acidic oxidative depolymerization prior to copolymerization with AN, a reference copolymer was synthesized using the original, non-depolymerized LB. This copolymer, poly(AN–LB)-17.5 (17.5 wt% LB), was directly compared with poly(AN–DLB)-17.5 (17.5 wt% DLB). Fig. 7A presents the molecular weight distributions of LB, DLB, PAN, and both copolymers. Notably, poly(AN–DLB)-17.5 exhibits a much higher molecular weight—reflected in its shorter elution time—than poly(AN–LB)-17.5. Specifically, M_w, M_n, and $Đ$ for poly(AN–LB)-17.5 were 32 688 g mol^{-1}, 15 588 g mol^{-1}, and 2.10, while the corresponding values for poly(AN–DLB)-17.5 were 161 975 g mol^{-1}, 81 868 g mol^{-1}, and 1.98. This substantial difference indicates that DLB promotes the formation of longer PAN chains compared to LB.

As previously discussed, LB and DLB differ significantly in their OHphen content (4.31 *vs.* 2.96 mmol g^{-1} for LB and DLB, respectively). This means that for the same lignin content in the formulation, LB provides more termination sites, which promotes earlier chain stopping and therefore shorter PAN

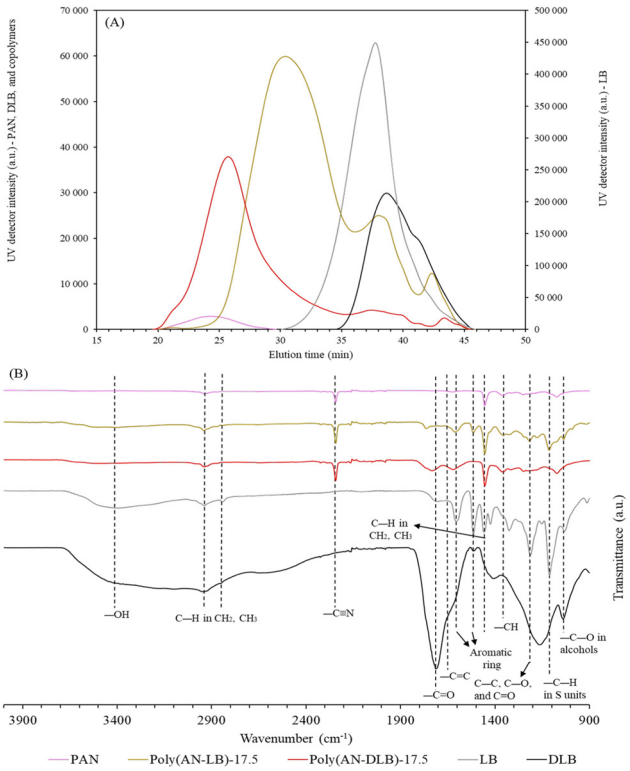

Fig. 7 (A) Molecular weight distribution and (B) ATR–FTIR spectra of PAN, poly(AN–LB)-17.5, poly(AN–DLB)-17.5, and DLB.

segments. At the molecular level, the difference is also evident: LB contains on average 2.74 reactive sites per molecule, whereas DLB contains approximately one (1.04). This lower density of reactive sites in DLB favors the formation of more linear architectures, as each molecule contributes roughly a single point where a PAN chain can graft. In contrast, the larger number of reactive sites in LB, as well as its bulkier molecular size, favors branching and limits the growth of long PAN chains, also due to steric hindrance. Overall, these results highlight the advantage of using DLB over LB: acidic oxidative depolymerization reduces the number of grafting/termination sites and relieves steric constraints, enabling the formation of higher-molecular-weight copolymers with more uniform and likely more linear structure. The higher UV intensity observed for LB relative to DLB may be attributed to its greater aromatic content and higher molecular weight.

Fig. 7B presents the ATR–FTIR spectra of both purified copolymers. Similar to poly(AN–DLB)-17.5, the poly(AN–LB)-17.5 copolymer exhibits functional groups derived from both PAN and lignin. The main differences between the two copolymers are as follows: poly(AN–DLB)-17.5 shows a C=O peak at 1710 cm^{-1}, associated with the oxidized character of DLB, whereas this peak is absent in poly(AN–LB)-17.5. Conversely, poly(AN–LB)-17.5 displays prominent signals characteristic of LB that are negligible in the DLB-based copolymer, including the peaks at 1515 cm^{-1} (aromatic ring vibration), 1213 cm^{-1} (C–C, C–O, and C=O linkages), and 1034 cm^{-1} (C–O in alco-

hols). Since LB contains a higher proportion of aromatic protons than DLB (26.9 *vs.* 4.1 wt% of total protons), these features are also reflected in their respective copolymers. For example, the peak at 1112 cm^{-1}—associated with C–H in S units and corresponding to in-plane aromatic C–H deformation—is present in both copolymers but appears significantly more intense in the one synthesized with LB. This is attributed to the partial degradation of aromatic side chains, such as OCH_3 groups, during the acidic oxidative depolymerization of LB to produce DLB. In both copolymers, the peaks at 2244 cm^{-1} and 1356 cm^{-1}—corresponding to C≡N stretching and C–H bending in CH groups, respectively—appear with strong intensity and are characteristic of PAN.

EA of the poly(AN–LB)-17.5 and poly(AN–DLB)-17.5 copolymers in terms of C, H, O, and S content (in percent) was performed (Table 6).

The EA results show that poly(AN–LB)-17.5 copolymer contains sulfur and oxygen, confirming the incorporation of LB into its structure, as these elements are present in LB but not in PAN. Furthermore, the high content of nitrogen detected in this copolymer can originate only from the PAN component, since its content in LB is extremely low.

The nitrogen content was also used to estimate the conversion and incorporation fraction of LB and AN. After the synthesis of poly(AN–LB)-17.5, the conversions of LB and AN were 53.1% and 36.1%, respectively, whereas for poly(AN–DLB)-17.5, the conversions of DLB and AN were 36.3% and 38.7%, respectively. The incorporation fraction of LB into the poly (AN–LB)-17.5 copolymer was 23.7%, while the incorporation fraction of DLB into poly(AN–DLB)-17.5 copolymer was 17.1%. The greater conversion and incorporation fraction of LB compared to DLB can be attributed to the higher content of phenolic OH groups in LB (Table 2), the activated sites in copolymerization. However, as discussed before, the phenolic OH content per mole of DLB, with only a single reactive site per molecule, is different from that in LB, which has 2.74 sites per molecule, which may promote the formation of a more linear copolymer. Indeed, the $Đ$ was lower for poly(AN–DLB)-17.5, indicating a more homogeneous copolymer.

The thermal behavior of poly(AN–LB)-17.5 was analyzed using TGA/DTG and DSC under both N_2 and air atmospheres. As shown in the DTG curve (Fig. 8A), a peak appears at approximately 100 °C, corresponding to the evaporation of residual moisture—similar to the behavior observed for poly

Table 6 Elemental analysis of PAN, poly(AN–LB)-17.5, poly(AN–DLB)-17.5, and DLB

Copolymers	Nitrogen (%)	Carbon (%)	Hydrogen (%)	Sulfur (%)	Oxygen (%)
PAN	25.92 ± 0.12	66.97 ± 0.18	5.96 ± 0.06	n.d.	n.d.
Poly(AN–LB)-17.5	19.79 ± 0.13	64.41 ± 0.09	6.11 ± 0.02	2.40 ± 0.07	7.30 ± 0.55
Poly(AN–DLB)-17.5	21.51 ± 0.05	61.57 ± 0.05	5.22 ± 0.06	0.21 ± 0.14	11.51 ± 0.20
LB	0.52 ± 0.33	57.99 ± 0.03	5.55 ± 0.02	3.10 ± 0.24	32.86 ± 0.06
DLB	0.02 ± 0.00	43.62 ± 0.07	3.77 ± 0.19	2.96 ± 0.01	49.63 ± 0.12

PAN: polyacrylonitrile, AN: acrylonitrile, LB: LignoBoost lignin, DLB: depolymerized LignoBoost lignin.

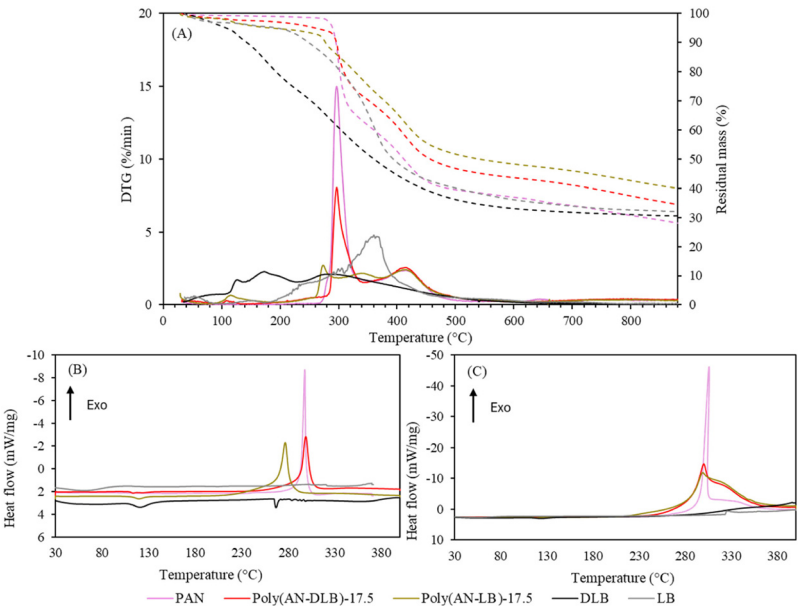

Fig. 8 Thermogravimetric analysis of PAN, poly(AN–LB)-17.5, poly(AN–DLB)-17.5, and DLB through (A) TGA, (B) DSC in N_2, and (C) DSC in air.

(AN–DLB)-17.5. After this initial stage, three distinct degradation peaks are observed: the first at 273 °C and the third at 420 °C, both characteristic of PAN, and a second peak at 350 °C, attributed to LB. In contrast, the poly(AN–DLB)-17.5 copolymer displayed only two major degradation peaks, closely resembling the thermal profile of PAN despite having almost the same lignin incorporation as poly(AN–LB)-17.5. This PAN-like behavior, absent in the poly(AN–LB)-17.5 sample, may be attributed to the heterogeneous nature of LB and to the longer PAN chains formed in poly(AN–DLB)-17.5. The higher molecular weight and structural complexity of LB likely hinder its dispersion within the copolymer matrix, making its influence on the thermal degradation profile more pronounced. The TGA curves (Fig. 8A) also show that poly(AN–LB)-17.5 exhibits greater initial mass loss compared to poly(AN–DLB)-17.5. However, its residual mass at 900 °C is higher (39.4 wt%) than that of poly(AN–DLB)-17.5 (33.8 wt%) and pure PAN (27.3 wt%). This enhanced char yield can be attributed to the higher aromatic content of LB, which leads to greater thermal residue and transfers this property to the corresponding copolymer.

The DSC analysis under N_2 (Fig. 8B) shows that the poly (AN–LB)-17.5 copolymer exhibits a sharp exothermic peak similar in shape to that of poly(AN–DLB)-17.5 but shifted to a lower temperature (T_{onset} of 206.2 °C *vs.* 227.8 °C). This suggests that the cyclization reaction initiates earlier in poly (AN–LB)-17.5, potentially due to the presence of shorter PAN chains. As previously discussed, the greater molecular weight and structural complexity of LB may exert a stronger influence on the thermal behavior of the copolymer. Moreover, its higher aromatic content likely contributes to improved thermal stability under inert conditions. Supporting this, ^{1}H NMR analysis (Fig. S7 of the SI) showed that aromatic protons accounted for 3.1% of total protons in poly(AN–LB)-17.5, com-

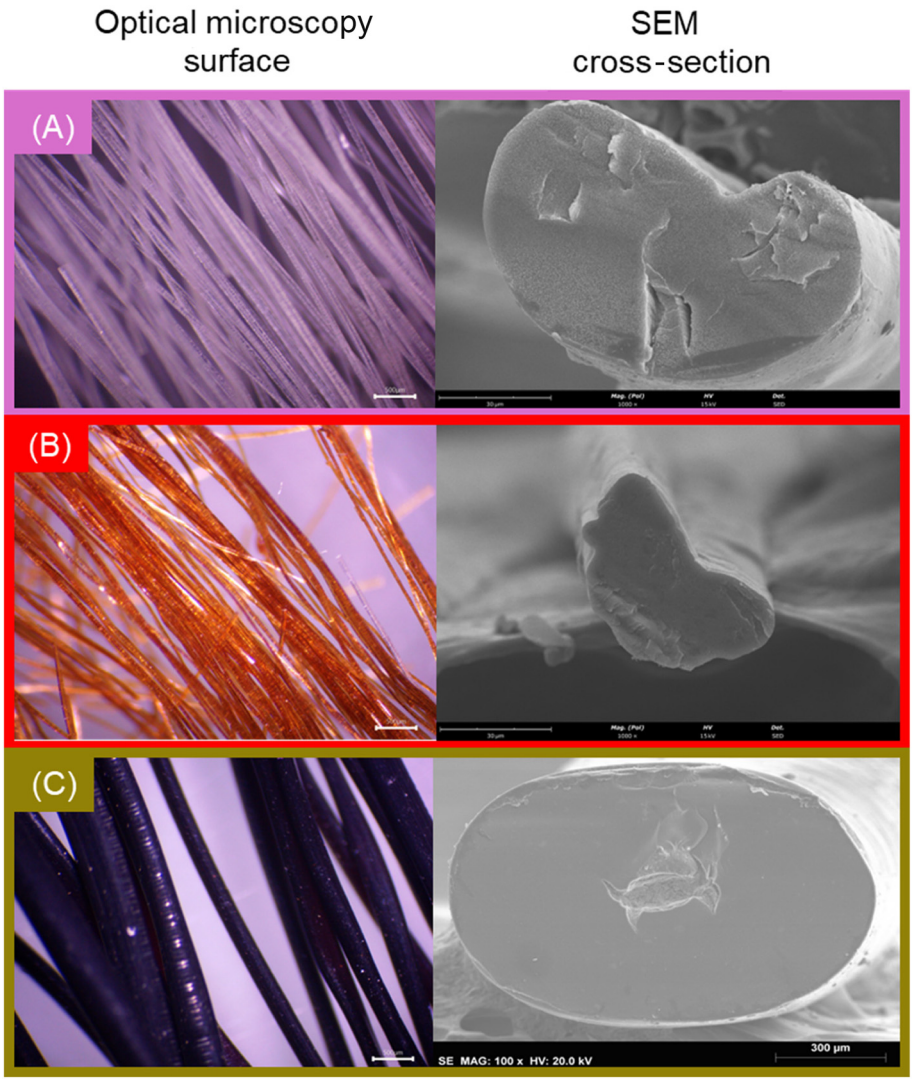

Fig. 9 Optical microscopy and SEM images of the surface and cross-sections of (A) poly(AN–VA), (B) poly(AN–DLB), and (C) poly(AN–LB). Scale bars: 500 µm for surface images and 1000 µm for cross-section images [except for the cross section of poly(AN–LB) that was 100×].

pared to only 0.2% in poly(AN–DLB)-17.5. A similar observation was reported by Oliveira *et al.* (2020), who found that lignin's large aromatic structures could lower the T_{onset} of cyclization reactions.[16]

Under an air atmosphere (Fig. 8C), the DSC curve of poly(AN–LB)-17.5 closely resembles that of poly(AN–DLB)-17.5, with overlapping exothermic events corresponding to cyclization and oxidation and a T_{peak} value of approximately 299.1 °C for both samples. This indicates that under oxidative conditions, the dominant thermal events are governed by oxidation reactions, which diminish the differences observed between the two copolymers under inert conditions.[38]

A comparative analysis of poly(AN–DLB)-17.5 and poly(AN–LB)-17.5 demonstrates that DLB is a more effective comonomer for producing copolymers with superior properties for fiber production. Poly(AN–DLB)-17.5 exhibited a likely more linear molecular structure, a significantly higher M_n (81 868 g mol^{-1} *vs.* 15 588 g mol^{-1}), and a lower $Đ$ (1.98 *vs.* 2.10), indicating a more homogeneous copolymer. Additionally, its thermal behavior more closely resembles that of PAN while offering advantages such as higher char yield and a more controlled and safer cyclization process, both critical for an efficient carbonization process.

3.5 Wet-spun fiber production

During wet spinning, the extrusion of the polymeric dope into the coagulation bath led to the rapid formation of solid fibers, driven by the diffusion exchange between the DMF and the aqueous coagulation medium. As shown in Fig. 9, optical microscopy of the surface and SEM images of the cross-sections confirm the successful continuous spinning and structural integrity of the as-spun fibers.

The poly(AN–VA) and poly(AN–DLB) fibers (Fig. 9A and B, respectively) exhibit smooth surfaces and dense cross-sectional morphologies. The average diameters were determined to be 80.96 ± 6.97 μm for poly(AN–VA) reference fibers and 56.94 ± 11.28 μm for poly(AN–DLB) fibers. Although some minor defects were observed on the cross-sections, likely artifacts induced by the cutting or fracturing process during sample preparation, the overall structure of the fibers remained predominantly dense and void-free. The successful production of these homogeneous continuous fibers confirms that the selected dope concentrations provided highly stable wet-spinning conditions.

In contrast, the poly(AN–LB) fibers (Fig. 9C) displayed a significantly larger and more heterogeneous average diameter (332.17 ± 70.08 μm). Notably, this diameter exceeds the dimension of the spinneret orifice (127 μm), indicating incomplete coagulation dynamics that led to the fusion (coalescence) of multiple adjacent filaments into a single, thicker structure. Furthermore, the resulting poly(AN–LB) fibers were highly brittle and prone to breakage, suggesting limited potential for achieving suitable mechanical performance.

Previous studies have reported that the incorporation of native lignin can simultaneously decrease the apparent viscosity of spinning dopes and increase their resistance to extensional deformation.[39,40] Both phenomena were observed in the poly(AN–LB) system, explaining the need for a significantly higher dope concentration and resulting in poorly stretched and fragile fibers. Conversely, the poly(AN–DLB) system minimized these rheological limitations. This improvement is attributed to the enhanced solubility and more uniform, linear chain conformation of the depolymerized lignin-based copolymers compared to the native lignin counterparts.

These findings highlight the critical role of lignin depolymerization prior to copolymer synthesis, as it enables the fabrication of lignin-based fibers with physical and morphological characteristics closely resembling those of commercial precursors.

4. Conclusions

This work demonstrates that depolymerized lignin can be incorporated directly into acrylonitrile-based copolymers using an aqueous free-radical copolymerization process, without the need for pre-functionalization using hazardous chlorinated acrylate intermediates and without azo-initiators. The resulting materials exhibit thermal stabilization behavior and structural characteristics compatible with the requirements for carbon fiber precursor development. While polyacrylonitrile was retained as a benchmark to enable comparison with established systems, the results clearly show that renewable content can be introduced without compromising key performance metrics. Depolymerized lignin led to the formation of lignin-based fibers with improved morphological characteristics compared with fibers produced from non-depolymerized lignin. This study represents a practical step toward reducing reliance on fossil-derived monomers and supports the development of safer and more sustainable carbon-fiber precursor platforms.

Author contributions

Talita Nascimento: writing – original draft, visualization, validation, methodology, investigation, formal analysis, and conceptualization. Marta Ramos-Andrés: writing – review & editing, visualization, validation, methodology, investigation, formal analysis, supervision, and conceptualization. Marta C. Lourenço: visualization, validation, methodology, investigation, formal analysis, and conceptualization. Ana C. Marques: writing – review & editing, visualization, supervision, project administration, methodology, funding acquisition, and conceptualization.

Conflicts of interest

There are no conflicts to declare.

Data availability

Data for this article are available at figshare at https://doi.org/10.6084/m9.figshare.30747215.

Supplementary information (SI) is available. See DOI: https://doi.org/10.1039/d6gc01695b.

Acknowledgements

The authors acknowledge Fundação para a Ciência e a Tecnologia (FCT) for financial support through the project BioCFiber, [2022.08091.PTDC, https://doi.org/10.54499/2022.08091.PTDC], the PhD fellowship 2024.02028.BDANA (T. N.), and CERENA Strategic Project funding FCT-UIDB/04028/2025 and FCT-UIDP/04028/2025. The authors also thank the European Union for support through the Horizon Europe Research and Innovation Program, Talent Pass (Grant Agreement No. 10121448, HORIZON-WIDERA-TALENTS-03), and RAIZ – Forest and Paper Research Institute for supplying LignoBoost lignin and black liquor. The authors gratefully acknowledge Inês Faria for contributions to the experimental work, Ivo Paulo for elemental analysis, Rui Dias for insightful discussions regarding industrial PAN-copolymer production, and José Paulo Farinha for the discussion regarding the mechanism of the reaction.

References

1 Y. Luo, W. Qu, E. Cochran and X. Bai, Enabling high-quality carbon fiber through transforming lignin into an orientable and melt-spinnable polymer, *J. Cleaner Prod.*, 2021, **307**, 127252, DOI: 10.1016/j.jclepro.2021.127252.

2 M. F. Hassan, M. A. Sabri, H. Fazal, A. Hafeez, N. Shezad and M. Hussain, Recent trends in activated carbon fibers production from various precursors and applications—A comparative review, *J. Anal. Appl. Pyrolysis*, 2020, **145**, 104715, DOI: 10.1016/j.jaap.2019.104715.

3 S. C. Sun, Y. Xu, J. L. Wen, T. Q. Yuan and R. C. Sun, Recent advances in lignin-based carbon fibers (LCFs): precursors, fabrications, properties, and applications, *Green Chem.*, 2022, **24**, 5709–5738, DOI: 10.1039/d2gc01503j.

4 W. Qu and X. Bai, Thermal treatment of pyrolytic lignin and polyethylene terephthalate toward carbon fiber production, *J. Appl. Polym. Sci.*, 2020, **137**, 1–10, DOI: 10.1002/app.48843.

5 Y. Wang, X. Meng, Y. Pu and A. J. Ragauskas, Recent Advances in the Application of Functionalized Lignin in Value-Added Polymeric Materials, *Polymers*, 2020, **12**, 1–24.

6 C. Banerjee, V. K. Chandaliya and P. S. Dash, Recent advancement in coal tar pitch-based carbon fiber precursor development and fiber manufacturing process, *J. Anal. Appl. Pyrolysis*, 2021, **158**, 105272, DOI: 10.1016/j.jaap.2021.105272.

7 F. Souto, V. Calado and N. Jr. Pereira, Lignin-based carbon fiber: a current overview, *Mater. Res. Express*, 2018, **5**(7), 072001, DOI: 10.1088/2053-1591/aaba00.

8 W. Qu, J. Yang, X. Sun, X. Bai, H. Jin and M. Zhang, Towards producing high-quality lignin-based carbon fibers: A review of crucial factors affecting lignin properties and conversion techniques, *Int. J. Biol. Macromol.*, 2021, **189**, 768–784, DOI: 10.1016/j.ijbiomac.2021.08.187.

9 W. Fang, S. Yang, X.-L. Wang, T.-Q. Yuan and R.-C. Sun, Manufacture and application of lignin-based carbon fibers (LCFs) and lignin-based carbon nanofibers (LCNFs), *Green Chem.*, 2017, **19**, 1794–1827, DOI: 10.1039/c6gc03206k.

10 S. C. Sun, Y. Xu, J. L. Wen, T. Q. Yuan and R. C. Sun, Recent advances in lignin-based carbon fibers (LCFs): precursors, fabrications, properties, and applications, *Green Chem.*, 2022, **24**, 5709–5738, DOI: 10.1039/d2gc01503j.

11 E. Zong, X. Liu, L. Liu, J. Wang, P. Song, Z. Ma, J. Ding and S. Fu, Graft Polymerization of Acrylic Monomers onto Lignin with $CaCl_2$-H_2O_2 as Initiator: Preparation, Mechanism, Characterization, and Application in Poly (lactic acid), *ACS Sustainable Chem. Eng.*, 2018, **6**, 337–348, DOI: 10.1021/acssuschemeng.7b02599.

12 H. Liu, Z. Dai, Q. Cao, X. Shi, X. Wang, H. Li, Y. Han, Y. Li and J. Zhou, Lignin/Polyacrylonitrile Carbon Fibers: The Effect of Fractionation and Purification on Properties of Derived Carbon Fibers, ACS Sustain, *Chem. Eng.*, 2018, **6**, 8554–8562, DOI: 10.1021/acssuschemeng.8b00868.

13 M.Ö Seydibeyolu, A novel partially biobased pan-lignin blend as a potential carbon fiber precursor, *J. Biomed. Biotechnol.*, 2012, **2012**, 598324, DOI: 10.1155/2012/598324.

14 X. Jiang, Q. Ouyang, D. Liu, J. Huang, H. Ma, Y. Chen, X. Wang and W. Sun, Preparation of low-cost carbon fiber precursors from blends of wheat straw lignin and commercial textile-grade polyacrylonitrile (PAN), *Holzforschung*, 2018, **72**, 727–734, DOI: 10.1515/hf-2017-0191.

15 M. S. Ganewatta, H. N. Lokupitiya and C. Tang, Lignin biopolymers in the age of controlled polymerization, *Polymers*, 2019, **11**(7), 1176, DOI: 10.3390/polym11071176.

16 T. S. Oliveira, T. R. Brazil, L. M. Guerrini, M. C. Rezende and M. P. Oliveira, Synthesis and characterization of poly (acrylonitrile-g-lignin) by semi-batch solution polymerization and evaluation of their potential application as carbon materials, *J. Polym. Res.*, 2020, **27**, 1–14, DOI: 10.1007/s10965-020-02318-8.

17 K. Xia, Q. Ouyang, Y. Chen, X. Wang, X. Qian and L. Wang, Preparation and Characterization of Lignosulfonate-Acrylonitrile Copolymer as a Novel Carbon Fiber Precursor, ACS Sustain, *Chem. Eng.*, 2016, **4**, 159–168, DOI: 10.1021/acssuschemeng.5b01442.

18 P. Liu, N. Zhang, Y. Yi, M. E. Gibril, S. Wang and F. Kong, Effect of lignin-based monomer on controlling the molecular weight and physical properties of the polyacrylonitrile/lignin copolymer, *Int. J. Biol. Macromol.*, 2020, **164**, 2312–2322, DOI: 10.1016/j.ijbiomac.2020.08.119.

19 W. J. Youe, S. M. Lee, S. S. Lee, S. H. Lee and Y. S. Kim, Characterization of carbon nanofiber mats produced from electrospun lignin-g-polyacrylonitrile copolymer, *Int. J. Biol. Macromol.*, 2016, **82**, 497–504, DOI: 10.1016/j.ijbiomac.2015.10.022.

20 S. P. Maradur, C. Hyo, S. Yeun, B. Kim, W. Chul and K. Seung, Preparation of carbon fibers from a lignin copoly-

mer with polyacrylonitrile, *Synth. Met.*, 2012, **162**, 453–459, DOI: 10.1016/j.synthmet.2012.01.017.

21 P. Porkodi, A. J. Kottiyatil and H. K. Shukla, A Novel method of controlling the molecular weight of PAN-lignin copolymer—Synthesis and characterization, *J. Mol. Struct.*, 2025, **1324**, 140694, DOI: 10.1016/j.molstruc.2024.140694.

22 N. Migliore, D. S. Zijlstra, T. G. Van Kooten, P. J. Deuss and P. Raffa, Amphiphilic Copolymers Derived from Butanosolv Lignin and Acrylamide: Synthesis, Properties in Water Solution, and Potential Applications, *ACS Appl. Polym. Mater.*, 2020, **2**, 5705–5715, DOI: 10.1021/acsapm.0c01006.

23 S. Jiang, D. Kai, Q. Q. Dou and X. J. Loh, Multi-arm carriers composed of an antioxidant lignin core and poly(glycidyl methacrylate-co-poly(ethylene glycol)methacrylate) derivative arms for highly efficient gene delivery, *J. Mater. Chem. B*, 2015, **3**, 6897–6904, DOI: 10.1039/c5tb01202c.

24 L. M. Steudle, E. Frank, A. Ota, U. Hageroth, S. Henzler, W. Schuler, R. Neupert and M. R. Buchmeiser, Carbon Fibers Prepared from Melt Spun Peracylated Softwood Lignin: an Integrated Approach, *Macromol. Mater. Eng.*, 2017, **302**, 1600441, DOI: 10.1002/MAME.201600441.

25 W. Qu, Y. Huang, Y. Luo, S. Kalluru, E. Cochran, M. Forrester and X. Bai, Controlled Radical Polymerization of Crude Lignin Bio-oil Containing Multihydroxyl Molecules for Methacrylate Polymers and the Potential Applications, *ACS Sustainable Chem. Eng.*, 2019, **7**, 9050–9060, DOI: 10.1021/acssuschemeng.9b01597.

26 B. Du, C. Chen, Y. Sun, M. Yang, M. Yu, B. Liu, X. Wang and J. Zhou, Unlocking the response of lignin structure by depolymerization process improved lignin-based carbon nanofibers preparation and mechanical strength, *Int. J. Biol. Macromol.*, 2020, **156**, 669–680, DOI: 10.1016/j.ijbiomac.2020.04.105.

27 T. Nascimento, M. Ramos-Andrés, R. Galhano dos Santos, A. Aguiar and A. C. Marques, A mild acidic oxidative process for lignin-derived functionalized monomers under catalyst, solvent, and pressure-free conditions, *Biomass Bioenergy*, 2025, **199**, 107949, DOI: 10.1016/j.biombioe.2025.107949.

28 M. C. Lourenço, T. Nascimento, P. J. S. Filho, A. C. Marques and M. Ramos-Andrés, Acidic Oxidative Depolymerization Towards Functionalized Low-Molecular-Weight Lignin and High-Value-Added Aliphatic Monomers: Operating Conditions, Scale-Up, and Crosslinking, *Int. J. Mol. Sci.*, 2025, **26**, 1–30, DOI: 10.3390/ijms26104872.

29 J. Sameni, S. Krigstin and M. Sain, Characterization of Lignins Isolated from Industrial Residues and their Beneficial Uses, *BioResources*, 2016, **11**, 8435–8456, DOI: 10.15376/biores.11.4.8435-8456.

30 X. Meng, C. Crestini, H. Ben, N. Hao, Y. Pu, A. J. Ragauskas and D. S. Argyropoulos, Determination of hydroxyl groups in biorefinery resources via quantitative 31P NMR spectroscopy, *Nat. Protoc.*, 2019, **14**, 2627–2647, DOI: 10.1038/s41596-019-0191-1.

31 A. More, T. Elder and Z. Jiang, A review of lignin hydrogen peroxide oxidation chemistry with emphasis on aromatic aldehydes and acids, *Holzforschung*, 2021, **75**, 806–823, DOI: 10.1515/hf-2020-0165.

32 Z. Ahmad, M. Paleologou and C. C. Xu, Oxidative depolymerization of lignin using nitric acid under ambient conditions, *Ind. Crops Prod.*, 2021, **170**, 113757, DOI: 10.1016/j.indcrop.2021.113757.

33 L. Falcão and M. E. M. Araújo, Application of ATR-FTIR spectroscopy to the analysis of tannins in historic leathers: The case study of the upholstery from the 19th century Portuguese Royal Train, *Vib. Spectrosc.*, 2014, **74**, 98–103, DOI: 10.1016/j.vibspec.2014.08.001.

34 N. L. T. Nguyen, C. Creighton, S. Nunna, M. Maghe, T. Groetsch and R. J. Varley, PAN-precursor to carbon fibre: An investigation of manufacture and material properties for varying comonomer composition, *Polym. Degrad. Stab.*, 2024, **227**, 110835, DOI: 10.1016/j.polymdegradstab.2024.110835.

35 G. Konstantopoulos, S. Soulis, D. Dragatogiannis and C. Charitidis, Introduction of a methodology to enhance the stabilization process of pan fibers by modeling and advanced characterization, *Materials*, 2020, **13**, 1–26, DOI: 10.3390/ma13122749.

36 N. Grassie and R. McGuchan, Pyrolysis of polyacrylonitrile and related polymers-IV. Thermal analysis of polyacrylonitrile in the presence of additives, *Eur. Polym. J.*, 1971, **7**, 1503–1514, DOI: 10.1016/0014-3057(71)90019-X.

37 P. Bajaj, T. V. Sreekumar and K. Sen, Thermal behaviour of acrylonitrile copolymers having methacrylic and itaconic acid comonomers, *Polymer*, 2001, **42**, 1707–1718, DOI: 10.1016/S0032-3861(00)00583-8.

38 W. J. Wang, S. Kharchenko, K. Migler and S. Zhu, Triple-detector GPC characterization and processing behavior of long-chain-branched polyethylene prepared by solution polymerization with constrained geometry catalyst, *Polymer*, 2004, **45**, 6495–6505, DOI: 10.1016/j.polymer.2004.07.035.

39 M. Al Aiti, A. Das, M. Kanerva, M. Järventausta, P. Johansson, C. Scheffler, M. Göbel, D. Jehnichen, H. Brünig, L. Wulff, S. Boye, K. Arnhold, J. Kuusipalo and G. Heinrich, Dry-jet wet spinning of thermally stable lignin-textile grade polyacrylonitrile fibers regenerated from chloride-based ionic liquids compounds, *Materials*, 2020, **13**(17), 3687, DOI: 10.3390/MA13173687.

40 H. Liu and H. Chung, Lignin-based polymers via graft copolymerization, *J. Polym. Sci., Part A:Polym. Chem.*, 2017, **55**, 3515–3528, DOI: 10.1002/pola.28744.

